POLYOXOMETALATES

Open Access
RESEARCH ARTICLE

Layered structured polyoxovanadate catalysts: Synthesis and performance in olefin epoxidation

Qichao Yan, Linmeng Lu, Jiawen Li, Ruikang Zhang, Yuanzhe Gao✉, Li Ma✉, and Zhan-Gang Han✉

Hebei Key Laboratory of Inorganic Nano-materials, National Demonstration Center for Experimental Chemistry Education, Hebei Engineering Research Center of Thin Film Solar Cell Materials and Devices, College of Chemistry and Material Science, Hebei Normal University, Shijiazhuang 050024, China

Cite This: *Polyoxometalates*, **2026**, *5*, 9140124

Read Online

ABSTRACT: Olefin epoxidation is a crucial transformation in organic synthesis, with significant applications in the pharmaceutical and fine chemical industries. The development of efficient catalysts that can use molecular oxygen as an environmentally benign oxidant under mild conditions remains a significant challenge. By employing diverse neutral ligands, two novel inorganic–organic hybrid polyoxovanadates were successfully synthesized: $[Zn^{II}(cyclam)(H_2O)][V^{V}_8O_{15}(OH)_{12}]$ (**1**) and $[Zn^{II}(phen)]_2[V^{V}_{12}O_{32}]\cdot H_2O$ (**2**) (cyclam = 1,4,8,11-tetraazacyclotetradecane, phen = 1,10-phenanthroline). The two compounds exhibit unique two-dimensional (2D) layered structural characteristics: compound **1** forms a wave-like 2D layer, whereas compound **2** exhibits a quasiplanar 2D extended structure. These structural features make the vanadium active centers more accessible to substrates, thereby significantly improving catalytic performance. Under optimized conditions, using molecular oxygen as the oxidant, compound **1** achieved a 99.9% conversion rate with 95.4% selectivity for the terminal alkene styrene at 50 °C and a 97.7% conversion rate with over 99% selectivity for the internal alkene cyclooctene at room temperature. Similarly, compound **2** also exhibited high catalytic activity. Compared with other catalysts reported in the literature, the two synthesized compounds exhibit excellent catalytic performance and stability under mild conditions and can be recycled multiple times without significant loss of activity. Structural analysis revealed that the 2D layered structures of these compounds provide additional accessible vanadium active sites, facilitating interactions between substrates and catalysts and thus enhancing catalytic efficiency.

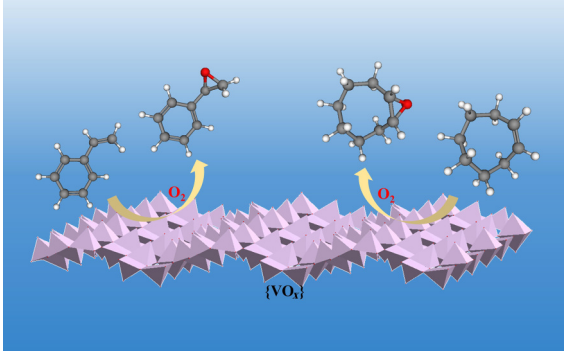

KEYWORDS: polyoxometalate, polyoxovanadate, inorganic-organic hybrid, epoxidation of olefin

1 Introduction

Polyoxometalates (POMs) are a class of nanoscale metal oxygen clusters formed by connecting MO_x polyhedra (M = Mo, W, V, *etc.*) through edge-, corner-, or face-sharing modes [1–5]. Because of their rich structural diversity and adjustable valence state characteristics, POMs have shown broad application prospects in many fields, such as magnetism, optics, catalysis, electronics, energy storage, and materials science [6–11]. Polyoxovanadates (POVs), an important branch of the POM family, have attracted significant attention because of their unique multivalent states and excellent redox properties [12–16]. Vanadium typically exhibits oxidation states of $V^{V/IV}$ (in some cases reaching $V^{III/II}$), and these different oxidation states can readily interconvert [17–20]. In contrast, Mo (primarily Mo^{VI}) and W (primarily W^{VI}) have singular oxidation states and more fixed coordination modes (mostly six-coordinated octahedral) [21–25]. Vanadium can form various coordination configurations, including tetrahedral (four-coordinated), square pyramidal (five-coordinated), and octahedral (six-coordinated) geometries. Furthermore, different coordination units (such as $\{VO_4\}$, $\{VO_5\}$, and $\{VO_6\}$) can flexibly connect to form various topological structures, including chains, layers, cages, and clusters [26–29]. As representative members of these compounds, the $\{V_8\}$ and $\{V_{12}\}$ clusters have been discovered and developed into various novel structures, providing strong support for the advancement of functional materials.

Figure 1(a) summarizes $\{V_8\}$ cluster structures reported in the literature [30–33]. These structures are clustered and exhibit excellent performance in carbon dioxide cycloaddition and sulfide catalytic oxidation. Figure 1(b) summarizes $\{V_{12}\}$ cluster structures reported in olefin epoxidation, sulfide catalytic oxidation, and other applications [34–38]. Despite the exceptional performance and application potential exhibited by the $\{V_8\}$ and $\{V_{12}\}$ clusters, the

Received: December 31, 2025; **Revised:** February 1, 2026
Accepted: February 19, 2026

✉Address correspondence to Yuanzhe Gao, yzgao@hebtu.edu.cn, yzgao2003@126.com; Li Ma, mali0801@hebtu.edu.cn; hanzg116@hebtu.edu.cn

https://doi.org/10.26599/POM.2026.9140124

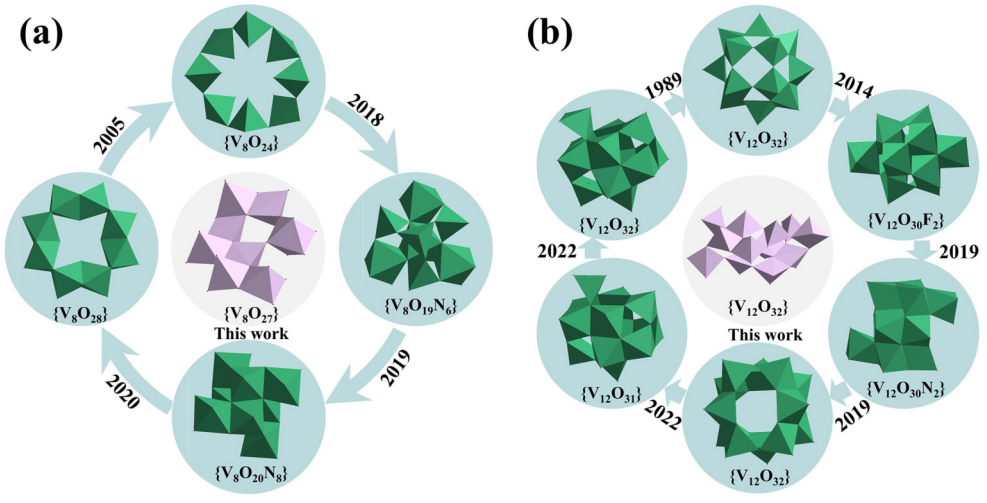

Figure 1 (a) The $\{V_8\}$ cluster structures. (b) The $\{V_{12}\}$ cluster structures.

structural diversity of these POVs in the literature remains scarce. The design and synthesis of new POV-based materials with enhanced functional properties remain challenging but crucial for advancing this field. Although the catalytic potential of POVs in oxidation reactions has been well established, their predominantly three-dimensional (3D) cluster configurations typically limit substrate accessibility to active sites, thereby reducing catalytic efficiency [39–43]. Therefore, the development of two-dimensional (2D) or planar POV structures can enhance substrate–catalyst interactions by increasing the surface area and active site exposure, thereby improving catalytic performance in heterogeneous systems.

Olefin epoxidation is an industrially significant transformation that produces valuable intermediates for fine chemicals and pharmaceuticals [44–47]. Conventional epoxidation methods typically rely on stoichiometric oxidants that generate substantial waste or require harsh reaction conditions [48]. Therefore, the development of efficient catalysts that can use molecular oxygen as the terminal oxidant under mild conditions is an important goal in sustainable chemistry. By leveraging the flexible intermediate oxidation states and redox properties of vanadium, coupled with its ability to form diverse spatial structures, the rational design of novel catalytic structures with optimized substrate binding sites and improved oxygen transfer efficiency becomes potentially feasible [49–51].

In this study, two new inorganic–organic hybrid POVs, namely, $\{V_8\}$ ($[Zn^{II}(cyclam)(H_2O)][V^{V}_8O_{15}(OH)_{12}]$ (**1**)) and $\{V_{12}\}$ ($[Zn^{II}(phen)]_2[V^{V}_{12}O_{32}]\cdot H_2O$ (**2**)) (cyclam = 1,4,8,11-tetraazacyclotetradecane, phen = 1,10-phenanthroline), were successfully synthesized. Unlike previously reported $\{V_8\}$ and $\{V_{12}\}$ clusters, compounds **1** and **2** exhibit unique structural features: compound **1** exhibits a distinctive wavy 2D layer, whereas compound **2** exhibits a novel quasiplanar 2D layer that extends outward. The structural features of these compounds, particularly their 2D architectures with accessible vanadium centers, contribute to their superior catalytic activity compared with conventional cage-like POM structures. The experimental results demonstrate that at 50 °C, using molecular oxygen as the oxidant, compound **1** achieves 99.9% conversion of terminal olefin styrene with 95.4% selectivity. At room temperature (25 °C), with O_2 as the oxidant, the conversion rate of internal olefin cyclooctene reaches 97.7% with > 99% selectivity. This study provides valuable insights into structure–activity relationships in POV catalysis and offers promising new catalytic systems for environmentally friendly olefin epoxidation.

2 Experimental

2.1 Experiment on catalytic reaction of olefin epoxidation

2.1.1 Styrene epoxidation

The catalytic activity of compounds **1** and **2** was systematically evaluated using a styrene reaction system with O_2. The reaction was conducted as follows: 2 mL of acetonitrile, 0.1 mmol of styrene, 25 mg of naphthalene (as an internal standard for gas chromatograph (GC) analysis), 2 mmol of isobutyraldehyde (IBA), and 10 mg of catalyst were successively added into a 25-mL vial. During the reaction, the vial was periodically replenished with O_2 every 10 min. The reaction was performed at 50 °C under stirring in a parallel reactor. The oxidation products of the olefin were analyzed via GC. Quantitative analysis was performed using the internal standard method. After the reaction, the catalyst was separated via centrifugation, washed several times with ethanol, and dried in air for reuse in recycling experiments.

2.1.2 Cyclooctene epoxidation

The catalytic activity of compounds **1** and **2** was also evaluated using a cyclooctene reaction system with O_2. The reaction was performed as follows: 2 mL of acetonitrile, 0.1 mmol of cyclooctene, 25 mg of naphthalene (as an internal standard), 2 mmol of IBA, and 5 mg of catalyst were successively added into a 25-mL vial. During the reaction, the vial was replenished with O_2 every 20 min. The reaction was performed at 25 °C under stirring in a parallel reactor. The oxidation products were analyzed by GC, and quantitative analysis was performed using the internal standard method. After the reaction, the catalyst was collected via centrifugation, washed several times with ethanol, and dried in air for subsequent recycling experiments.

3 Results and discussion

3.1 Synthesis and structures of compounds 1 and 2

Hydrothermal synthesis is a common approach for POVs even

though obtaining novel structures requires careful control of key parameters, including pH value, reaction temperature, and metal salt type. Systematic studies have demonstrated that compound **1** crystallizes within the pH range of 3.3–3.9, whereas compound **2** crystallizes at a pH of approximately 5.2. The reaction temperature is also crucial. The best crystals can be obtained at 160 °C. When the reaction temperature drops to 140 °C, compound **1** cannot be obtained, whereas compound **2** yields rough-surfaced crystals with a significant decrease in yield. In addition, the type of metal salt affects crystal formation. When other types of metal salts are used, the target product cannot be obtained. For compound **2**, if GeO_2 is not added, the target crystal cannot be formed. It is speculated that GeO_2 plays a structural guide role in the synthesis process.

3.2 Crystal structures of compounds 1 and 2

Single-crystal X-ray diffraction (SCXRD) analysis indicates that compound **1** crystalizes in the *Pnma* space group of the orthorhombic crystal system, and its basic structural unit is composed of a $[V^{V}_{8}O_{15}(OH)_{12}]^{2-}$ anion cluster and a $[Zn(cyclam)]^{2+}$ unit (Fig. 2(a)). The anionic cluster structure units of **1** are simple but interesting, and the vanadium in it has different coordination modes, including $\{VO_5\}$ and $\{VO_6\}$. The adjacent $\{VO_5\}$ tetragonal pyramids with shared edges exhibit different orientations, resulting in a smaller steric hindrance effect and making the structure more stable. In compound **1**, Zn^{2+} is located in a hexa-coordinated octahedral environment, coordinated by one O atom in H_2O, four N atoms of one cyclam ligand, and one O atom of an anion cluster. The oxidation states of V and Zn were determined as +V and +II, respectively, using the bond valence sum (BVS) method (Table S3 in the Electronic Supplementary Material (ESM)). In compound **1**, $[Zn(cyclam)]^{2+}$ is interconnected with the layer surface oxygen through covalent bonds (Fig. 2(b)). The structural units can form 2D layered structures by connecting $\{VO_5\}$ and $\{VO_6\}$ through shared edges or corners. The $\{V_8\}$ anion cluster forms a 2D pure inorganic vanadium oxide layer on the *ab* plane (Fig. 2(c)). The interlaced arrangement of ligands connecting different layers was discovered through the 3D stacking structure, thereby achieving effective space utilization (Fig. 2(d)). Layers are connected through N–H···O hydrogen bonds to form a 3D supramolecular framework (Fig. S1 in the ESM).

Compound **2** crystallizes in the *C*2/*m* space group of the monoclinic crystal system. Its basic structural unit comprises the $[V^{V}_{12}O_{32}]^{4-}$ anion cluster, two $[Zn(phen)]^{2+}$ units, and one crystalline water (Fig. 3(a)). The anion cluster comprises two $\{V_6O_{16}\}$ units in different directions, which are connected by shared $\{VO_4\}$ corners to form a binuclear cluster structure. In compound **2**, $[Zn(phen)]^{2+}$ is interconnected with the layer surface oxygen through covalent bonds, and Zn^{2+} is located in a hexa-coordinated octahedral environment, which is coordinated by two N atoms of one phen ligand and four O atoms of the anion cluster. The oxidation states of V and Zn were determined as +V and +II, respectively, by BVS (Table S3 in the ESM). The $\{V_{12}\}$ anion cluster forms 2D inorganic vanadium oxide chains on the *bc* plane (Fig. 3(b)). By stacking 3D structures, ligands connected by different layers are interlaced, achieving effective utilization of space (Figs. 3(c) and 3(d)). These layers are connected through C–H···O hydrogen bonds to form a 3D supramolecular framework (Fig. S2 in the ESM).

For compound **1** (Fig. 4(a)), the peaks at 516.6 and 523.8 eV belong to V^{V} $3p_{3/2}$ and V^{V} $3p_{1/2}$, respectively, indicating pure oxidation states. The peaks at 1021.0 and 1044.1 eV belong to Zn^{II} $3p_{3/2}$ and Zn^{II} $3p_{1/2}$, respectively (Fig. 4(b)). For compound **2** (Fig. 4(c)), the peaks at 517.1 and 524.4 eV belong to V^{V} $3p_{3/2}$ and

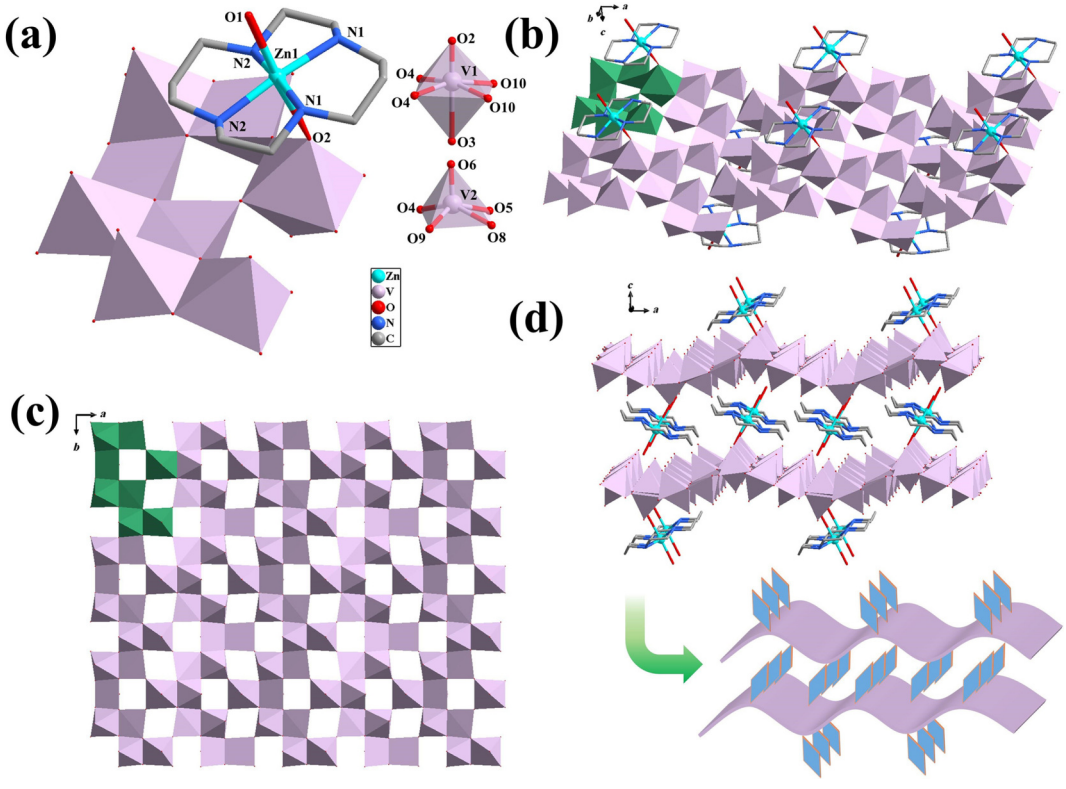

Figure 2 (a) The structural unit of compound **1**. (b) 2D layered structure of compound **1**. (c) The 2D layer structure of the anionic cluster structure of compound **1**. (d) 3D stacked structure and abstract structure of compound **1**.

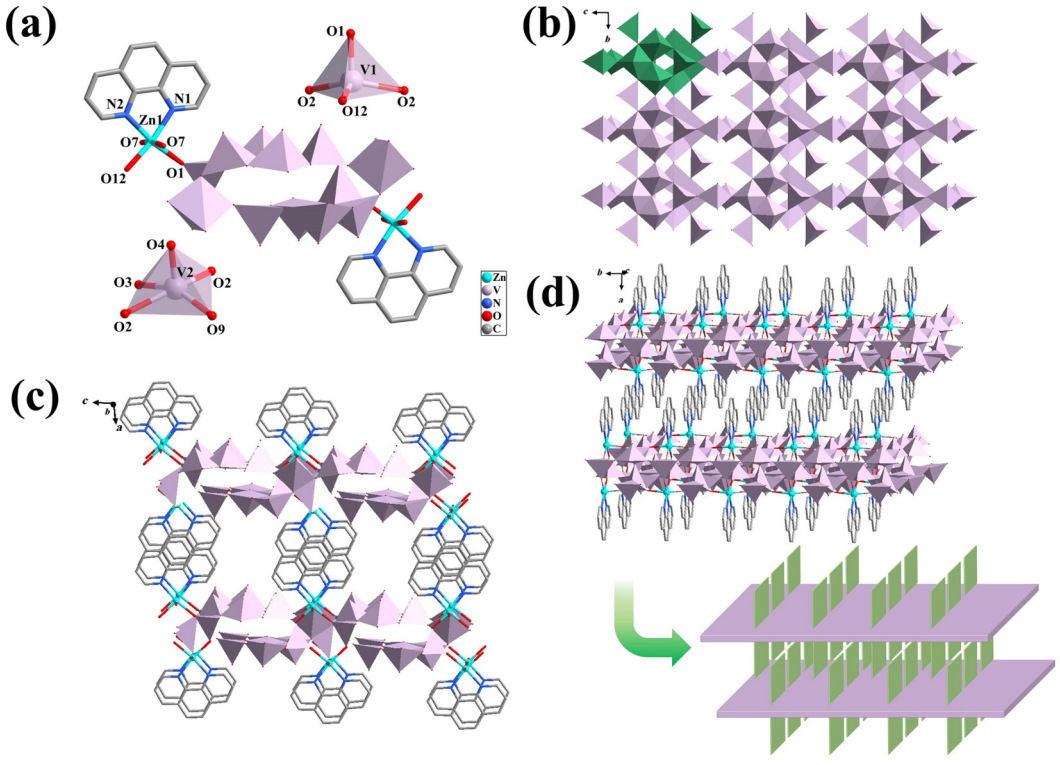

Figure 3 (a) The structural unit of compound **2**. (b) 2D layered structure of compound **2**. (c) 3D stacked structure of compound **2**. (d) 3D stacked structure and abstract structure of compound **2**.

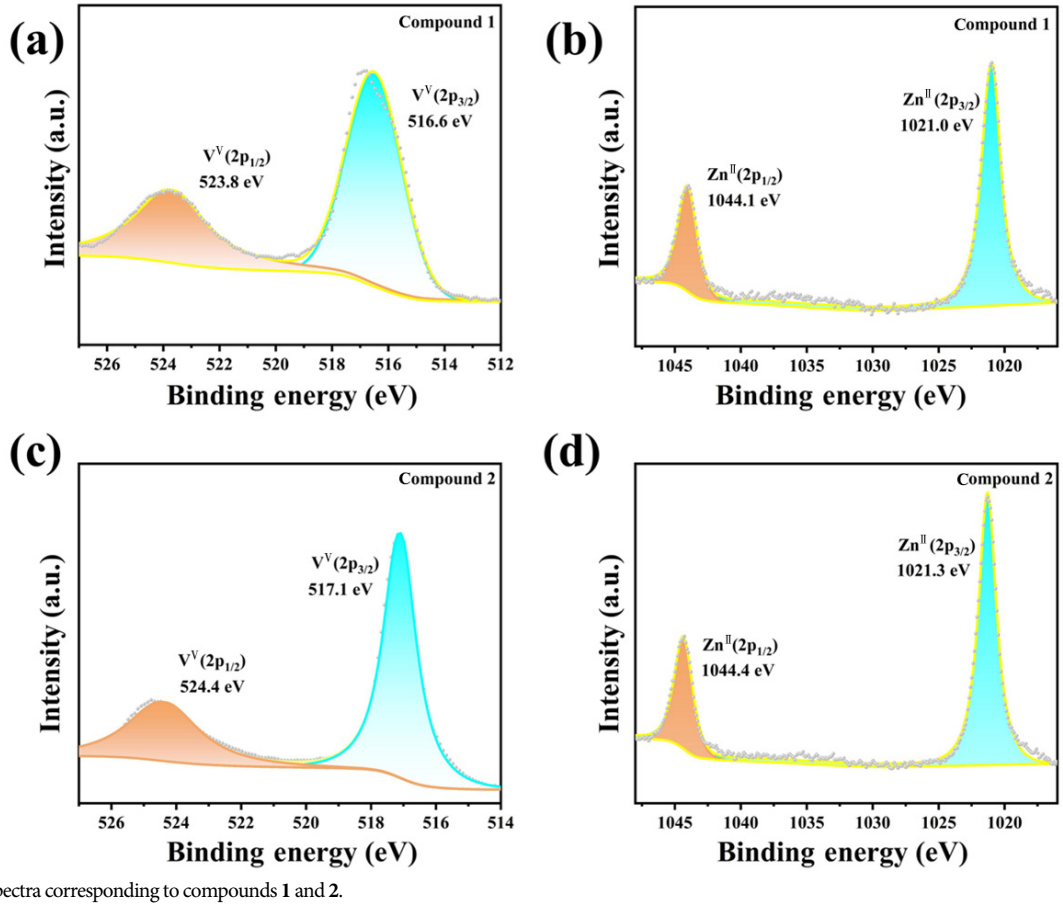

Figure 4 XPS spectra corresponding to compounds **1** and **2**.

V^{V} $3p_{1/2}$, respectively, representing pure oxidation states. The peaks at 1021.3 and 1044.4 eV belong to Zn^{II} $3p_{3/2}$ and Zn^{II} $3p_{1/2}$, respectively (Fig. 4(d)). The test results are consistent with the BVS calculations [52]. The simulated and experimental powder X-ray diffraction (PXRD) patterns of compounds **1** and **2** are shown in Fig. S4 in the ESM. The experimental and simulated PXRD patterns of the two compounds are consistent, confirming that they exist as pure phases.

4 Catalytic oxidation reaction

4.1 Catalytic activities of compounds 1 and 2 in styrene epoxidation

Olefin epoxidation produces highly reactive epoxides with extensive applications in the synthesis of fine chemicals and pharmaceutical intermediates. The use of environmentally benign molecular oxygen as an oxidant presents significant challenges for catalyst design and performance. Because of the presence of Lewis acid active sites and redox properties in POV clusters, they can be used as highly efficient catalysts for olefin oxidation. Owing to their 2D planar structures, compounds **1** and **2** offer distinct advantages over cage-like POM clusters by providing greater accessibility to active sites, potentially enhancing their catalytic performance. In this study, styrene was selected as a model substrate to evaluate the catalytic properties of both compounds. Preliminary catalytic screening revealed that compound **1** exhibited superior catalytic activity compared with compound **2**. Consequently, compound **1** was selected as the preferred catalyst for the detailed investigation of styrene epoxidation reactions.

Systematic screening was performed to investigate the influence of reaction temperature. The results demonstrated that styrene conversion reached its maximum at 50 °C. Further increases in the reaction temperature did not significantly improve the conversion rate; however, the selectivity of styrene oxidation decreased (Fig. 5(a)). Conversely, when the temperature approached room temperature, the conversion rate dropped significantly. Subsequently, the influence of catalyst dosage was also investigated (Fig. 5(b)). At a catalyst dosage of 5 mg, the conversion rate of styrene was 89.2%. An increase in the catalyst dosage to 10 mg provided additional active sites, thereby enhancing styrene conversion. The influence of IBA concentration on styrene epoxidation was also investigated. Multiple experimental trials revealed that 2 mmol of IBA was the optimal concentration (Fig. S6 in the ESM). Subsequently, the reaction solvent was also optimized, and acetonitrile exhibited the highest conversion rate as a solvent (Fig. 5(c)). Finally, to deeply explore the primary active sites in compound **1**, a series of control experiments was conducted using the precursors of compound **1** as catalysts based on optimal catalytic reaction conditions (Fig. 5(d)).

The optimal reaction conditions for styrene epoxidation were as follows: styrene (0.1 mmol), catalyst (10 mg), solvent acetonitrile (2 mL), IBA (2 mmol), O_2 (1 atm), temperature (50 °C), and reaction time (40 min). Under these optimized conditions, the

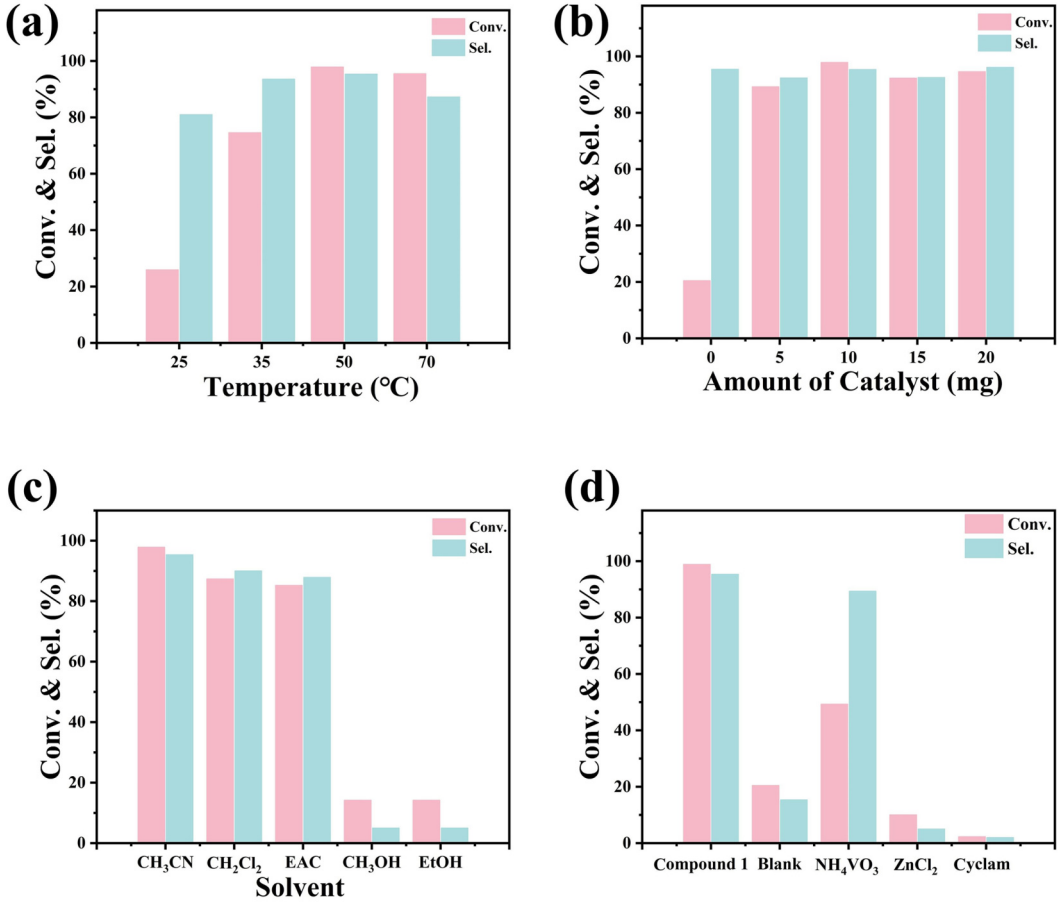

Figure 5 The impact of various parameters on reaction activity: (a) reaction temperature; (b) the amount of catalyst; (c) in different solvents; (d) the catalytic oxidation reaction of styrene with different catalysts.

styrene epoxidation experiment was conducted using compounds **1** and **2** as catalysts. Compound **1** exhibited exceptional catalytic performance, achieving 99.9% conversion with 95.4% selectivity within 40 min (Fig. 6(a)). Compound **2** exhibited slightly lower efficiency with 99.8% conversion and 91.1% selectivity under identical conditions (Fig. 6(b)).

In addition, by expanding the substrate types, the universal applicability and effect of compound **1** in the catalytic system were verified. Considering the excellent catalytic performance of compound **1**, the catalytic activity of styrene derivatives was further investigated. Styrene derivatives with electron-withdrawing groups (e.g., –F and –Cl) were oxidized to the corresponding epoxides, achieving high conversion rates (96.8% and 96.5%, respectively) and selectivity (94.5% and 95.6%, respectively; Table 1, entries 2 and 3, respectively). Styrene derivatives with electron-donating groups (e.g., $–CH_3$, $–OCH_3$) exhibit excellent conversion rates (98.9% and 99.9%, respectively), whereas the selectivity of the corresponding epoxides drops to 92.3% and 93.5%, respectively (Table 1, entries 4 and 5, respectively). Among the two groups, the electron-donating group exhibits an electron-donating effect through conjugation, increasing the electron density on C=C and enhancing reactivity, thereby reducing epoxide selectivity. In conclusion, compound **1** exhibits outstanding catalytic performance for various terminal alkenes.

Subsequently, under the optimal catalytic conditions, cyclic experimental tests were conducted with compound **1** (Fig. 7). After each reaction, the catalyst was recovered by centrifugation and washed with ethanol. The conversion rate of the reaction did not significantly decrease in the five-cycle experiment. In addition, no significant changes were observed in the Fourier transform infrared (FTIR) spectra and PXRD patterns before and after the reaction, indicating that the cycling stability of compound **1** was excellent. The thermal filtration test was conducted with the $\{V_8\}$ catalyst for the ring oxidation reaction of styrene. After the reaction lasted for 10 min, the solution was recovered via centrifugal filtration to remove the catalyst and then subjected to another 30 min of reaction under the same conditions. No significant increase in the yield was observed after the catalyst was removed, indicating that the $\{V_8\}$ catalyst has heterogeneous characteristics (Fig. S7 in the ESM).

Table S4 in the ESM summarizes recently reported precious metal heterogeneous materials (entry 1), polymetallic oxides (entries 2 and 7–9), metal–organic frameworks and their composites (entries 3, 4, and 6), and non-metallic materials (entry 5) as catalysts for styrene epoxidation reactions. In catalytic oxidation experiments, catalyst selection should follow the nonpollution and nonrisk principles. Therefore, the use of oxygen as an oxidant is the ideal choice. Among entries 1–3 oxygen is used as the oxygen source. Furthermore, catalytic styrene oxidation involves the oxidation of products such as styrene, benzaldehyde, and benzoic acid. Among these products, oxidized styrene has the highest application value and serves as an important intermediate in chemical synthesis. In entries 5–7 in Table S4 in the ESM, the main product of this series of catalysts is benzaldehyde, whereas the products in the other entries are styrene oxide. Finally, these types of catalysts have limitations such as relatively high reaction temperatures, long reaction times, and low product selectivity (Table S4 in the ESM). In comparison, compounds **1** and **2** feature moderate reaction temperatures, shorter reaction times, and higher conversion rates and selectivity, thereby standing out among numerous catalysts (entries 10 and 11 in Table S4 in the ESM). Compared with cage-type cluster configurations, the 2D layered structures of compounds **1** and **2** offer increased accessibility to vanadium active sites, thereby strengthening substrate–catalyst interactions and improving catalytic efficiency.

4.2 Catalytic activities of compound 1 in cyclooctene epoxidation

Following previous studies on terminal alkene epoxidation, this section explores cyclic olefin transformation reactions. In cyclooctene epoxidation, compound **1** performed exceptionally well as a catalyst, operating effectively at room temperature. To further demonstrate the epoxidation performance of olefins, compound **1** was evaluated as a catalyst with cyclooctene serving as a model substrate. Through comprehensive experiments, the optimal reaction parameters were established, and the principal factors influencing its catalytic efficiency were examined.

In an O_2 atmosphere, the influence of different reaction temperatures on the reaction was evaluated (Fig. S8(a) in the ESM). The results demonstrate that at 25 °C, the conversion rate of cyclooctene is high. In addition, the effect of catalyst amount on the reaction was investigated (Fig. S8(b) in the ESM). When 5 mg of catalyst was used, the conversion rate of cyclooctene was 97.7%. The effect of IBA loading on cyclooctene epoxidation was also examined (Fig. S8(c) in the ESM), and analysis of multiple datasets indicated that the optimal IBA dosage was 2 mmol. Similarly, the reaction solvent was also optimized, and the highest conversion rate was obtained using acetonitrile as the solvent (Fig. 8(a)). To further investigate the key active sites in compound **1**, control experiments were conducted using the precursor of compound **1** as the catalyst under optimal catalytic conditions (Fig. 8(b)).

The optimal reaction conditions for cycloalkene epoxidation

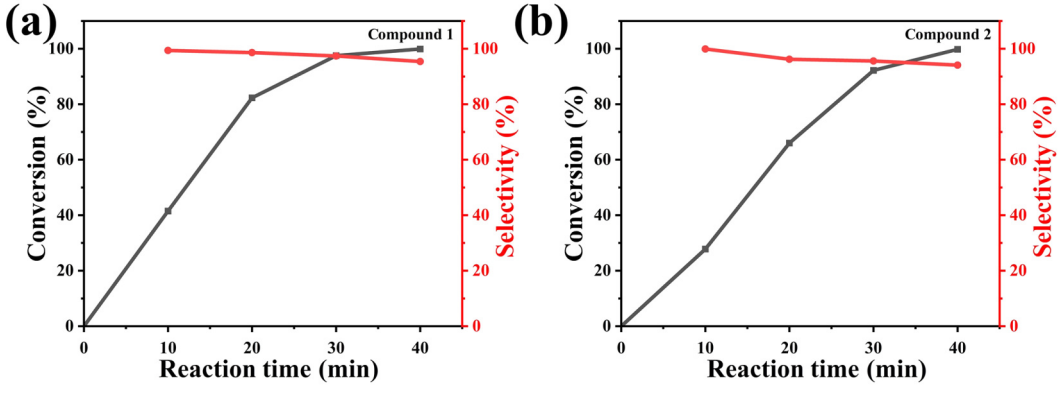

Figure 6 (a) Catalytic performance of compound **1** under optimal reaction conditions. (b) catalytic performance of compound **2** under optimal reaction conditions.

Table 1 The conversion and selectivity of different styrene derivatives by compound **1**[ab]

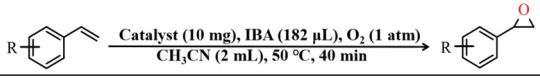

Entry	Substrate	Production	Time (min)	Conv. (%)	Sel. (%)
1			40	99.9	95.4
2	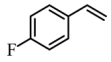	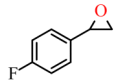	40	96.8	94.5
3	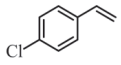	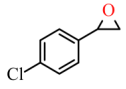	40	96.5	95.6
4	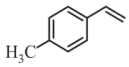	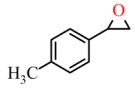	40	98.9	92.3
5	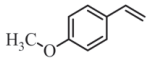	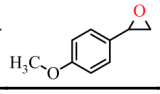	40	99.9	93.5

[a]Reaction conditions: temperature (50 °C), CH_3CN (2 mL), styrene (0.1 mmol), O_2 (1 atm), catalyst **1** (10 mg), IBA (2 mmol), and reaction time (40 min). [b]Determined by GC analysis.

were determined as follows: acetonitrile solvent (2 mL), substrate (0.1 mmol), catalyst (5 mg), IBA (2 mmol), O_2 (1 atm), temperature (25 °C), and reaction time (2 h). The conversion rate of compound **1** is 97.7%, and the selectivity is > 99% (Fig. S9 in the ESM).

Given the exceptional catalytic efficacy of compound **1**, its activity was subsequently evaluated across diverse olefinic substrates. The test results demonstrate that cycloalkenes with smaller steric hindrance are more prone to reaction than those with larger steric hindrance. When compound **1** was used to catalyze cyclopentene and cyclohexene, the conversion efficiency of cyclopentene and cyclohexene reached 92.9% and 95.7%, respectively, after 2 h (Table 2, entries 2 and 3, respectively). The conversion rates of both substrates decreased compared with the oxidation of cyclooctene. This phenomenon is attributed to the lower C=C bond dissociation energies in cyclopentene and cyclohexene than in cyclooctene. In contrast, norbornene achieves a conversion efficiency of 91.5% (Table 2, entry 4). When indene and trans-stilbene with higher steric hindrance were selected, the conversion rate decreased significantly (19.1% and 13.2%, respectively; Table 2, entries 5 and 6, respectively). In conclusion, compound **1** demonstrates outstanding catalytic performance and broad applicability in the epoxidation of various cyclic alkenes.

Compound **1** exhibited excellent recyclability and robust stability over five reaction cycles (Fig. 9). Even after repeated recovery via centrifugation and ethanol washing, no significant decrease in conversion was observed. The structural stability of the catalyst was verified by FTIR and PXRD analyses, which showed no notable changes in the post-reaction material. Similarly, a thermal filtration experiment was conducted. After 40 min of the reaction, the catalyst was removed by centrifugation, and the filtrate was allowed

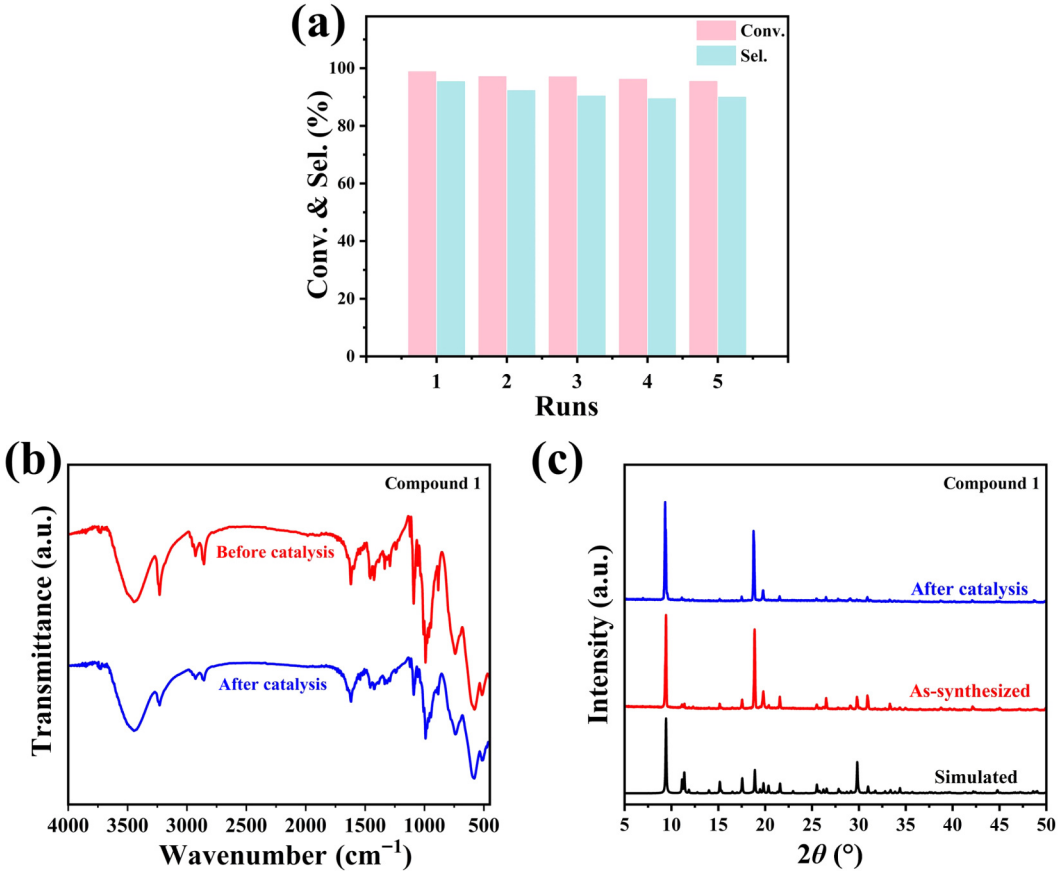

Figure 7 (a) Five consecutive reuse cycles for compound **1** in the styrene epoxidation. (b) The FTIR spectra of the cycled compound **1** following its reuse in the styrene epoxidation. (c) The PXRD patterns of the cycled compound **1** following its reuse in the styrene epoxidation.

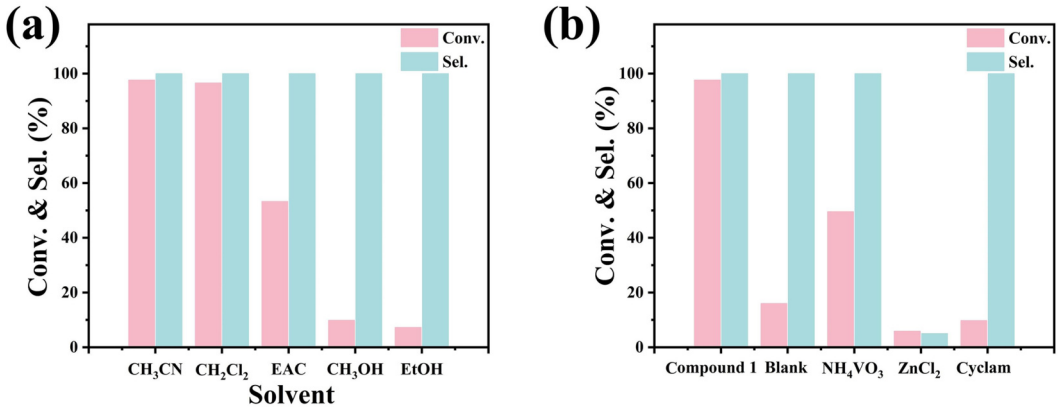

Figure 8 (a) and (b) The impact of various parameters on reaction activity: (a) in different solvents; (b) the catalytic oxidation reaction of cyclooctene with different catalysts.

Table 2 The conversion and selectivity of different cyclooctene derivatives by compound **1**[ab]

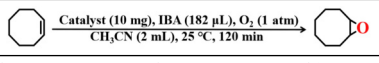

Entry	Substrate	Production	Time (h)	Conv. (%)	Sel. (%)
1			2	97.7	99
2			2	92.9	99
3			2	95.7	99
4			2	91.5	99
5			2	19.1	99
6	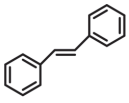	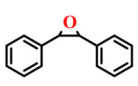	2	13.2	—

[a]Reaction conditions: temperature (25 °C), CH_3CN (2 mL), cyclooctene (0.1 mmol), O_2 (1 atm), catalyst **1** (5 mg), IBA (2 mmol), and reaction time (2 h). [b]Determined by GC analysis.

to react for an additional 80 min under the same conditions. The results demonstrated that the yield did not significantly increase after the catalyst was removed, confirming the heterogeneous catalytic nature of the $\{V_8\}$ catalyst (Fig. S10 in the ESM).

Table S5 in the ESM summarizes recently reported metal hydroxides (entry 2), multimetal oxides (entries 3, 9, 11, and 12), metal–organic frameworks and their composites (entries 1, 4, 5, and 7), and non-metallic materials (entry 8) as catalysts for cyclooctene epoxidation. Although the cyclooctene epoxidation reaction generally exhibits high selectivity, its efficient progress typically depends on harsh conditions above room temperature. Compound **1** can efficiently catalyze reactions at 25 °C in the absence of light systems. The mild catalytic conditions of compound **1** highlight its unique application potential and research value (entries 13 and 14). In contrast to cage cluster structures, the 2D layered architectures of the synthesized compounds provide a higher number of accessible vanadium active sites, facilitating effective interactions between catalysts and substrates and consequently improving catalytic performance.

Using compound **1** as a model catalyst, the possible mechanism of alkene epoxidation was investigated (Fig. 10). During the catalytic process, IBA is adsorbed onto the $\{V^V_8\}$ surface. Due to the presence of IBA, V^V is reduced to V^{IV}, which is accompanied by the formation of an isobutyryl radical. Subsequently, V^{IV} is re-oxidized to V^V by molecular oxygen, generating a $\cdot O_2^-$ radical species. The isobutyryl radical reacts with the $\cdot O_2^-$ radical to form peroxyisobutyric acid anions. The alkene is then oxidized by these peroxyisobutyric acid anions to produce the corresponding epoxide, thereby completing the catalytic cycle. Finally, the catalyst is regenerated and re-enters the next catalytic cycle, demonstrating the efficient redox mechanism underlying the epoxidation process.

5 Conclusions

In this study, two novel layered isopolyoxovanadates were successfully synthesized using the hydrothermal method. The structures of the two compounds were characterized using SCXRD. Unlike conventional 3D cage-like POV clusters, both compounds exhibited unique 2D layered structures, which significantly expanded the structural diversity of POV clusters. Compound **1** demonstrated excellent catalytic activity in the catalytic oxidation experiments of terminal and cyclic alkenes under mild conditions, using environmentally benign and readily available molecular oxygen (O_2) as the oxidant source. This outstanding performance can be attributed to the variable valence state of vanadium and its distinctive layered structure that provides additional accessible active sites. The catalyst demonstrated high conversion rates, excellent selectivity, and significant stability in olefin epoxidation experiments. This study provides meaningful insights into the design and research of POV-based catalysts in the field of efficient epoxidation of terminal and internal olefins with green oxidants.

Electronic Supplementary Material: Supplementary material (experimental section, crystallographic data, bond lengths and angles, BVS calculation data, supplementary structure figures, IR spectra, PXRD patterns, TG curves, EPR spectrum) is available in the online version of this article at https://doi.org/10.26599/POM.2026.9140124.

CCDC 2514693-2514694 contain the supplementary crystallographic data for this paper.

Data availability

All data needed to support the conclusions in the paper are presented in the manuscript and the Electronic Supplementary Material. Additional data related to this paper may be requested from the corresponding author upon request.

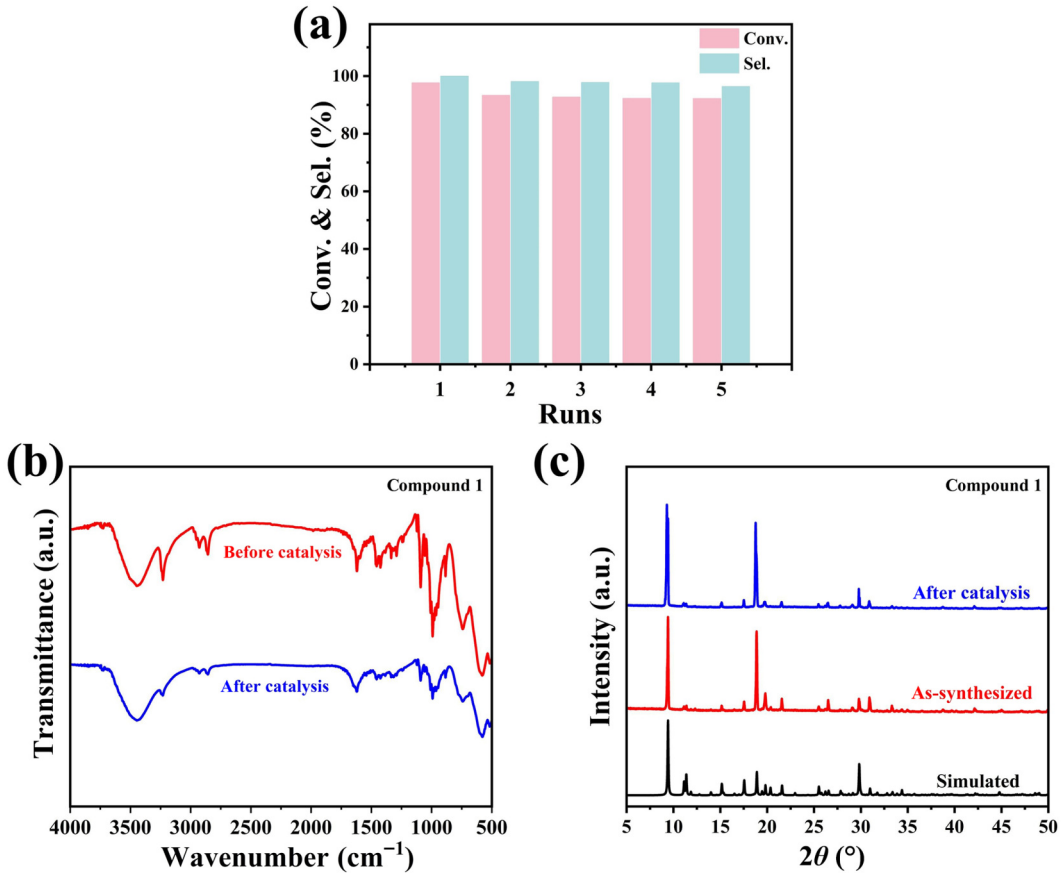

Figure 9 (a) Five consecutive reuse cycles for compound **1** in the epoxidation of cyclooctene. (b) The FTIR spectra of the cycled compound **1** following its reuse in the epoxidation of cyclooctene. (c) The PXRD patterns of the cycled compound **1** following its reuse in the epoxidation of cyclooctene.

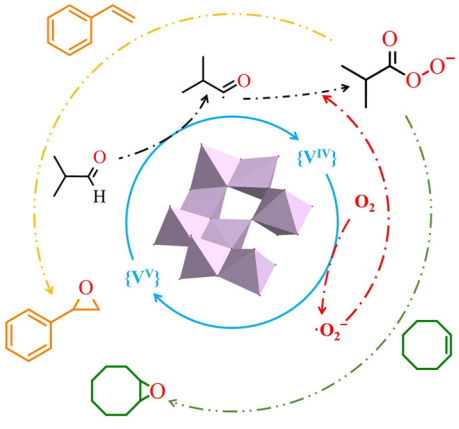

Figure 10 The possible catalytic mechanism of compound **1** in catalytic epoxidation of cyclooctene or styrene.

Acknowledgements

This work was supported by the Natural Science Foundation of Hebei Province (Nos. B2021205027 and B2024205033), the National Natural Science Foundation of China (No. 22371065), and Science Foundation of Hebei Normal University (L2025K02).

Declaration of competing interest

The authors have no competing interests to declare that are relevant to the content of this article. Author Zhan-Gang Han is the editorial board member of this journal, but he is not involved in the peer-review or decision of this article.

Author contribution statement

Q. C. Y.: Data curation, formal analysis, investigation, writing – original draft. L. M. L.: Data curation, validation. J. W. L.: Experiment, validation. R. K. Z.: Supervision, data curation. Y. Z. G.: Project administration, data curation, funding acquisition, supervision, writing – review & editing. L. M.: Funding acquisition, data curation, writing – review & editing. Z.-G. H.: Project administration, funding acquisition, writing – review & editing. All the authors have approved the final manuscript.

Use of AI statement

None.

References

[1] Lin, J. L.; Zheng, A.; Xie, Y.; Chen, N. Y.; He, R. L.; Yin, B. C.; Lv, W. K.; Wei, Y. G.; Li, Y. Transition from tunneling to schottky barriers in molecular junctions based on polyoxometalate monolayers. *Angew. Chem., Int. Ed.* **2025**, *64*, e202501763.

[2] Liu, J.; Jiang, N.; Lin, J. M.; Mei, Z. B.; Dong, L. Z.; Kuang, Y.; Liu, J. J.; Yao, S. J.; Li, S. L.; Lan, Y. Q. Structural evolution of giant polyoxometalate: From "keplerate" to "lantern" type Mo_{132} for improved oxidation catalysis. *Angew. Chem., Int. Ed.* **2023**, *62*, e202304728.

[3] Ng, M. T. K.; Bell, N. L.; Long, D. L.; Cronin, L. Facile and reproducible electrochemical synthesis of the giant polyoxomolybdates. *J. Am. Chem. Soc.* **2021**, *143*, 20059–20063.

[4] Zhang, D.; Wang, C. G.; Lin, Z. G.; Dong, L. Z.; Zhang, C.; Yao, Z. S.; Lei, P.; Dong, J.; Du, J. X.; Chi, Y. N. et al. Fullerene-like niobovanadate cage built from {(Nb)V_5} pentagon. *Angew. Chem., Int. Ed.* **2024**, *63*, e202320036.

[5] Ma, X. Y.; Bi, H. X.; Zhang, X. J.; Du, J.; Ma, Y. Y.; Han, Z. G. Effect of bridging units on the detection performance of Cd{P_4Mo_6}$_2$-based electrochemical sensors for trace chromium(VI) and tetracycline. *Polyoxometalates* **2025**, *4*, 9140090.

[6] Zhu, Q.; Li, Z. H.; Zheng, T.; Zheng, X. X.; Liu, S.; Gao, S.; Fu, X. H.; Su, X. F.; Zhu, Y.; Zhang, Y. M. et al. High-selectivity tandem photocatalytic methanation of CO_2 by lacunary polyoxometalates-stabilized *CO intermediate. *Angew. Chem., Int. Ed.* **2025**, *64*, e202413594.

[7] Kong, H.; Ma, P. T.; Wang, J. P.; Niu, J. Y. Overview of organophosphonate covalently modified polyoxometalates: From synthesis and structural diversity to applications. *Polyoxometalates* **2025**, *4*, 9140103.

[8] Li, Y. R.; Li, Z.; Li, J.; Liu, T. F.; Lv, H. J.; Yang, G. Y. Decatungstate-based photocatalysts for organic transformations. *Polyoxometalates* **2025**, *4*, 9140101.

[9] Hu, B.; Liu, B. L.; Pan, Q. Q.; Ren, H. D.; Yu, F. Y.; Du, Q. C.; Li, Y. G.; Zang, H. Y. Structural effects in polyoxometalate-based supramolecular assemblies for enhanced proton conduction. *Angew. Chem., Int. Ed.* **2026**, *65*, e17958.

[10] Wang, J. J.; Wu, Z. Y.; Li, Q.; Zhang, H. L.; Liu, Y.; Ji, G. X.; Zhang, Y. L.; Li, Q. L.; Ren, J. Y.; Zhang, Q. D. et al. Engineering boron-imidazolate-based polyoxometalates for photooxidative C=C bond cleavage in aqueous media. *Polyoxometalates* **2025**, *4*, 9140087.

[11] Zhu, Z. K.; Lin, Y. Y.; Yu, H.; Li, X. X.; Zheng, S. T. Inorganic-organic hybrid polyoxoniobates: Polyoxoniobate metal complex cage and cage framework. *Angew. Chem., Int. Ed.* **2019**, *131*, 17020–17024.

[12] Lu, L. M.; Hu, Z. Y.; Yan, Q. C.; Gao, X. Y.; Liu, C. N.; Zhang, R. K.; Ma, L.; Gao, Y. Z. Two new isopolyoxovanadates based on V_{10} and V_6: Structural assembly and dual catalytic applications. *Inorg. Chem. Front.* **2025**, *12*, 7845–7854.

[13] Wang, J. L.; Cao, J. P.; Zhu, Y. H.; Wang, Q. Li, N. F.; Fan, X. R.; Mei, H.; Xu, Y. Four unprecedented V_{14} clusters as highly efficient heterogeneous catalyst for CO_2 fixation with epoxides and oxidation of sulfides. *Sci. China Chem.* **2023**, *66*, 107–116.

[14] Dang, T. Y.; Li, R. H.; Tian, H. R.; Wang, Q.; Lu, Y.; Liu, S. X. Tandem-like vanadium cluster chains in a polyoxovanadate-based metal-organic framework for efficient catalytic oxidation of sulfides. *Inorg. Chem. Front.* **2021**, *8*, 4367–4375.

[15] Monakhov, K. Y.; Bensch, W.; Kögerler, P. Semimetal-functionalised polyoxovanadates. *Chem. Soc. Rev.* **2015**, *44*, 8443–8483.

[16] Müller, A.; Krickemeyer, E.; Penk, M.; Rohlfing, R.; Armatage, A.; Bögge, H. Template-controlled formation of cluster shells or a type of molecular recognition: Synthesis of $[HV_{22}O_{54}(ClO_4)]^{6-}$ and $[H_2V_{18}O_{44}(N_3)]^{5-}$. *Angew. Chem., Int. Ed.* **1991**, *30*, 1674–1677.

[17] Li, J.; Zhang, D.; Chi, Y. N.; Hu, C. W. Catalytic application of polyoxovanadates in the selective oxidation of organic molecules. *Polyoxometalates* **2022**, *1*, 9140012.

[18] Wang, K.; Xu, Q. F.; Ma, P. T.; Zhang, C.; Wang, J. P.; Niu, J. Y. Polyoxovanadate catalysts for oxidation of 1-phenyl ethanol: From the discrete $[V_4O_{12}]^{4-}$ and $[V_{10}O_{28}]^{6-}$ anions to the anionic $[V_6O_{17}]_n^{4n-}$ coordination polymer. *CrystEngComm* **2018**, *20*, 6273–6279.

[19] Chen, M.; He, C. H.; Liu, Q.; Deng, W. Z.; Sun, C. F. A mass-producible polyoxovanadate cathode for ultrafast-kinetics zinc-ion batteries. *Inorg. Chem. Front.* **2024**, *11*, 3643–3652.

[20] Guo, W. W.; Bacsa, J.; van Leusen, J.; Sullivan, K. P.; Lv, H. J.; Kögerler, P.; Hill, C. L. A layered manganese(IV)-containing heteropolyvanadate with a 1:14 stoichiometry. *Inorg. Chem.* **2015**, *54*, 10604–10609.

[21] Zhang, J. W.; Huang, Y. C.; Li, G.; Wei, Y. G. Recent advances in alkoxylation chemistry of polyoxometalates: From synthetic strategies, structural overviews to functional applications. *Coord. Chem. Rev.* **2019**, *378*, 395–414.

[22] Gu, Q. X.; Zhao, X. L.; Meng, M.; Shao, Z. Y.; Zheng, Q.; Xuan, W. M. Crystalline porous ionic salts assembled from polyoxometalates and cationic capsule for the selective photocatalytic aerobic oxidation of aromatic alcohols to aldehydes. *Chin. Chem. Lett.* **2023**, *34*, 107444.

[23] Song, N. Z.; Lu, M. Y.; Liu, J. C.; Lin, M.; Ping, S. G.; Wang, J. F.; Shi, B. Y.; Zhao, J. W. A giant heterometallic polyoxometalate nanocluster for enhanced brain-targeted glioma therapy. *Angew. Chem., Int. Ed.* **2024**, *63*, e202319700.

[24] Feng, Y. Q.; Fu, F. Y.; Zeng, L. L.; Zhao, M. Y.; Xin, X.; Liang, J. K.; Zhou, M.; Fang, X. K.; Lv, H. J.; Yang, G. Y. Atomically precise silver clusters stabilized by lacunary polyoxometalates with photocatalytic CO_2 reduction activity. *Angew. Chem., Int. Ed.* **2024**, *63*, e202317341.

[25] Junkers, L. S.; Garay-Ruiz, D.; Builds, J.; Silberg, R. S.; Strapasson, G. B.; Jensen, K. M. Ø.; Bo, C. Uncovering polyoxometalate speciation in hydrothermal systems by combining computational simulation with X-ray total scattering. *J. Am. Chem. Soc.* **2025**, *147*, 22747–22758.

[26] Müller, A.; Rohlfing, R.; Döring, J.; Penk, M. Formation of a cluster sheath around a central cluster by a "self-organization process": The mixed valence polyoxovanadate $[V_{34}O_{82}]^{10-}$. *Angew. Chem., Int. Ed.* **1991**, *30*, 588–590.

[27] Lühmann, H.; Näther, C.; van Leusen, J.; Kögerler, P.; Bensch, W. Three intersecting {V_{12}} rings: {$V_{30}Sb_8$}, an ultra-large polyoxovanadate cluster shell. *Chem. Commun.* **2021**, *57*, 7661–7664.

[28] Liu, C. N.; Shi, Y.; Yan, Q. C.; Lu, L. M.; Ma, L.; Zhang, R. L.; Lin, Z. G.; Gao, Y. Z. Transition metal-modified {$V_{14}Sb_8$}-type polyoxovanadates: Reusable catalysts for Knoevenagel condensation under mild conditions. *J. Mol. Struct.* **2026**, *1352*, 144490.

[29] Liu, S. Y.; He, Y. Z.; Ma, X. Y.; Liu, J. Y.; Ma, P. T.; Wang, J. P.; Niu, J. Y. Synthesis and structure of high-nuclearity carboxylate-modified heteropolyoxovanadate serving as a heterogeneous catalyst for selective oxidation of alkylbenzenes. *Inorg. Chem.* **2023**, *62*, 18384–18390.

[30] Kurata, T.; Uehara, A.; Hayashi, Y.; Isobe, K. Cyclic polyvanadates incorporating template transition metal cationic species: Synthesis and structures of hexavanadate $[PdV_6O_{18}]^{4-}$, octavanadate $[Cu_2V_8O_{24}]^{4-}$, and decavanadate $[Ni_4V_{10}O_{30}(OH)_2(H_2O)_6]^{4-}$. *Inorg. Chem.* **2005**, *44*, 2524–2530.

[31] Inoue, Y.; Kodama, S.; Taya, N.; Sato, H.; Oh-Ishi, K.; Ishii, Y. Reductive formation of a vanadium(IV/V) oxide cluster complex $[V_8O_{19}(4,4'\text{-}^t\text{Bubpy})_3]$ having a C_3-symmetric propeller-shaped nonionic V_8O_{19} core. *Inorg. Chem.* **2018**, *57*, 7491–7494.

[32] Cao, J. P.; Xue, Y. S.; Li, N. F.; Gong, J. J.; Kang, R. K.; Xu, Y. Lewis acid dominant windmill-shaped V_8 clusters: A bifunctional heterogeneous catalyst for CO_2 cycloaddition and oxidation of sulfides. *J. Am. Chem. Soc.* **2019**, *141*, 19487–19497.

[33] Ping, Q. D.; Cao, J. P.; Han, M. Y.; Yang, M. X.; Hong, Y. L.; Li, J. N.; Wang, J. L.; Chen, J. L.; Mei, H.; Xu, Y. Eight-membered ring petal-shaped V_8 cluster: An efficient heterogeneous catalyst for selective sulfur oxidation. *Inorg. Chim. Acta* **2021**, *517*, 120198.

[34] Day, V. W.; Klemperer, W. G.; Yaghi, O. M. Synthesis and characterization of a soluble oxide inclusion complex, $[CH_3CN\subset(V_{12}O_{32}^{4-})]$. *J. Am. Chem. Soc.* **1989**, *111*, 5959–5961.

[35] Krivosudský, L.; Schwendt, P.; Gyepes, R.; Filo, J. $[V_{12}O_{30}F_4(H_2O)_2]^{4-}$: One-pot synthesis and characterization of a novel fluorinated dodecavanadate. *Inorg. Chem. Commun.* **2014**, *49*, 48–51.

[36] Nicolaou, M.; Drouza, C.; Keramidas, A. D. Controlled one pot synthesis of polyoxofluorovanadate molecular hybrids exhibiting peroxidase like activity. *New J. Chem.* **2019**, *43*, 17595–17602.

[37] Lu, H. J.; Jethwa, R. B.; Jenkinson, K. J.; Wheatley, A. E. H.; Hao, H.

X.; Wright, D. S.; Pike, S. D. A simple one-step synthetic route to access a range of metal-doped polyoxovanadate clusters. *Dalton Trans.* **2019**, *48*, 4555–4564.
[38] Kikukawa, Y.; Sakamoto, Y.; Hirasawa, H.; Kurimoto, Y.; Iwai, H.; Hayashi, Y. Synthesis and oxidation catalysis of a difluoride-incorporated polyoxovanadate and isolation of active vanadium alkylperoxo species. *Catal. Sci. Technol.* **2022**, *12*, 2438–2445.
[39] Fertig, A. A.; Brennessel, W. W.; McKone, J. R.; Matson, E. M. Concerted multiproton-multielectron transfer for the reduction of O_2 to H_2O with a polyoxovanadate cluster. *J. Am. Chem. Soc.* **2021**, *143*, 15756–15768.
[40] Kato, N.; Hayashi, Y. Discrete spherical hexadecavanadates incorporating a bromide with oxidative bromination activity. *Dalton Trans.* **2013**, *42*, 11804–11811.
[41] Huang, X. Q.; Liu, S.; Liu, G.; Tao, Y. W.; Wang, C. R.; Zhang, Y. L.; Li, Z.; Wang, H. W.; Zhou, Z.; Shen, G. D. et al. An unprecedented 2-fold interpenetrated ***lvt*** open framework built from Zn_6 ring seamed trivacant polyoxotungstates used for photocatalytic synthesis of pyridine derivatives. *Appl. Catal. B: Environ.* **2023**, *323*, 122124.
[42] Li, G.; Wang, X. M.; Pang, H. J.; Ma, H. Y. Molecular weaving of mixed-addenda polyoxometalates into MOF nanochannels as electron-buffering reservoirs for enhanced nitrate-to-ammonia electrocatalysis. *Adv. Sci*., in press, DOI: 10.1002/advs.202521317.
[43] Zhang, Y. L.; Su, X. F.; Zheng, T.; Shah, W. A.; Yan, L. K.; Li, S. J. Flexible intervention of polyoxometalate support on the electronegativity of single atoms to enhance catalytic activity. *Inorg. Chem.* **2025**, *64*, 3824–3830.
[44] Xie, H. R.; Li, H.; Xiao, J. P. Recent progress in electrocatalytic epoxidation of alkenes. *Curr. Opin. Electrochem.* **2025**, *53*, 101733.
[45] Nunes, C. D.; Calhorda, M. J. Molybdenum(II) catalyst precursors in olefin oxidation reactions. *Inorg. Chim. Acta* **2015**, *431*, 122–131.
[46] Lee, E. Y.; Shuler, M. L. Molecular engineering of epoxide hydrolase and its application to asymmetric and enantioconvergent hydrolysis. *Biotechnol. Bioeng.* **2007**, *98*, 318–327.
[47] Choi, W. J.; Choi, C. Y. Production of chiral epoxides: Epoxide hydrolase-catalyzed enantioselective hydrolysis. *Biotechnol. Bioprocess Eng.* **2005**, *10*, 167–179.
[48] Zhang, H. D.; Zou, Y.; Wang, Y. M.; Shen, Y.; Zheng, X. X. Asymmetric epoxidation of *cis*/*trans*-*β*-methylstyrene catalysed by immobilised Mn(Salen) with different linkages: Heterogenisation of homogeneous asymmetric catalysis. *Chem.—Eur. J.* **2014**, *20*, 7830–7841.
[49] Zhang, Z. Y.; Lin, Q. P.; Kurunthu, D.; Wu, T.; Zuo, F.; Zheng, S. T.; Bardeen, C. J.; Bu, X. H.; Feng, P. Y. Synthesis and photocatalytic properties of a new heteropolyoxoniobate compound: $K_{10}[Nb_2O_2(H_2O)_2][SiNb_{12}O_{40}]\cdot 12H_2O$. *J. Am. Chem. Soc.* **2011**, *133*, 6934–6937.
[50] Zhao, Q. X.; Zeng, Y.; Jiang, Z. Q.; Huang, Z. X.; Long, D. L.; Cronin, L.; Xuan, W. M. High-nuclearity polyoxometalate-based metal-organic frameworks for photocatalytic oxidative cleavage of C–C bond. *Angew. Chem., Int. Ed.* **2024**, *64*, e202421132.
[51] Chen, J. L.; Shen, Q. B.; Jing, X.; Duan, C. Y. Design of pyridine tetracarboxylate-bridged polyoxometalate-based metal-organic framework for photocatalytic oxidative amine coupling and *α*-amino C(sp^3)-H arylation. *Inorg. Chem.* **2025**, *64*, 12022–12030.
[52] Silversmit, G.; Depla, D.; Poelman, H.; Marin, G. B.; de Gryse, R. Determination of the V2p XPS binding energies for different vanadium oxidation states (V^{5+} to V^{0+}). *J. Electron Spectrosc. Relat. Phenom.* **2004**, *135*, 167–175.

Yuanzhe Gao received her Ph.D. degree from Beijing Institute of Technology in 2010. In 2015, she worked as a visiting scholar at Emory University in USA. Her current research focuses on the construction and catalytic properties of polyoxometalates, particularly polyoxovanadates. She has published over 50 papers in important international academic journals.

Li Ma received her Ph.D. degree from Northeast Normal University in 2019. Currently working at the College of Chemistry and Materials Science, Hebei Normal University. Research focuses on the design, synthesis, and property investigation of functionalized inorganic-organic hybrid materials.

Zhan-Gang Han received his Ph.D. degree from Northeast Normal University in 2005. In 2010–2011, he worked as a university teacher-visiting scholar at two universities in Monash University and The University of New South Wales, Australia. His current research interests focus on the construction of novel polyoxometalate structures and their photo-electrochemistry research. In 2016, he was funded by the Outstanding Youth Fund of Hebei Province and was selected as the third-level candidate for the "Three-Three-Three Talents Project" in Hebei Province. He has published more than 100 papers in important international academic journals.